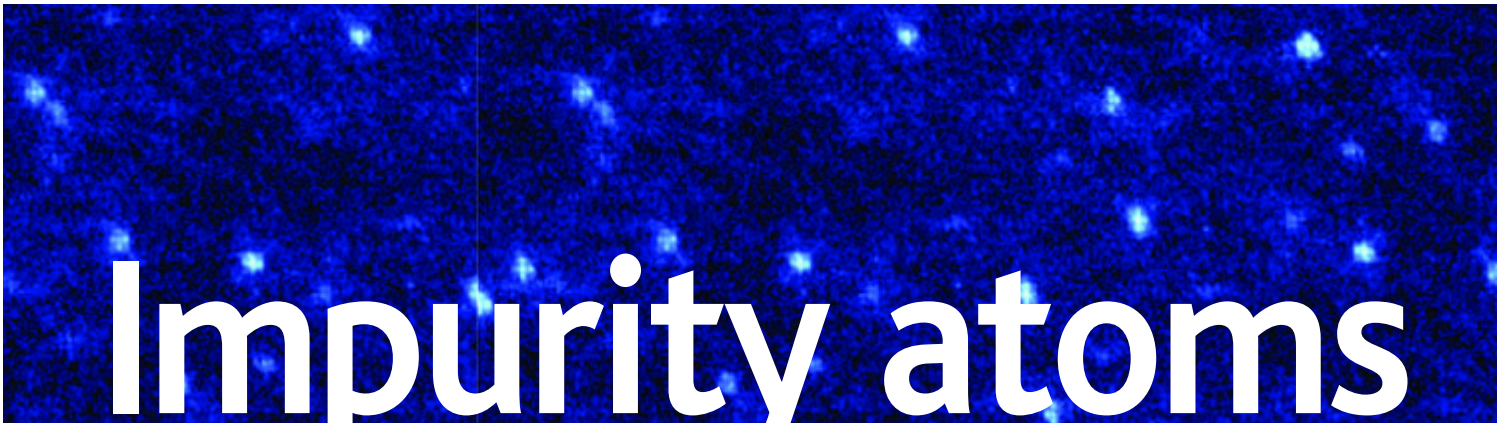

Impurity atoms on view in cuprates

by J.C. Séamus Davis

Impurity atoms in a material are usually viewed as a problem because they can result in non-ideal properties. However, they can sometimes be used to advantage when attempting to understand new materials. This is because the interactions of an impurity atom with the material reveal detailed information on the local electronic environment. In this paper we discuss scanning tunneling microscopy studies of the atomic-scale effects of individual Ni and Zn impurity atoms on the cuprate high critical temperature superconductors.

Department of Physics,
University of California, Berkeley,
CA 94720, USA
Email: jcdavis@socrates.berkeley.edu

Conventional superconductors

Bardeen-Cooper-Schrieffer (BCS) theory provides a microscopic picture of how attractive electron-electron interactions in the degenerate electron gas of a metal result in the formation of Cooper-pairs[1]. Each Cooper-pair can be considered a bound state of two electrons with opposite spin and momentum. The superconducting ground-state then essentially represents condensation of these Cooper-pairs into a single macroscopic quantum state – a process analogous to Bose-Einstein condensation. In conventional superconductors, the order parameter (OP) associated with this BCS ground-state typically has s-wave symmetry.

The formation of Cooper-pairs opens a gap of width Δ in the density of electronic states at the Fermi level. This is referred to as the superconducting energy gap. Above this gap, a new spectrum of excited states called Bogoliubov quasiparticles appears. Near the Fermi level, these quasiparticles have a density of states and dispersion relation very different from those of the Landau quasiparticles of the metallic parent state. They are of central interest here because single particle tunneling experiments can be used to measure the energy dependence of their density of states[2].

Cuprate superconductors

Among the best known cuprate high-critical temperature (T_c) superconductors (HTS) are the compounds $La_{2-x}Sr_xCuO_4$, $YBa_2Cu_3O_{7-x}$, $Bi_2Sr_2CaCu_2O_{8+x}$, $Tl_2Ba_2Ca_2Cu_3O_{10}$, and $HgBa_2Ca_3Cu_4O$. All of these materials contain one or more crystal planes per unit cell consisting of only Cu and O atoms in a square lattice. Superconductivity originates from the strongly interacting electrons in these CuO_2 planes. The Cu atoms are believed to be in the Cu^{2+} $3d^9$ configuration with

ISSN:1369 7021 © Elsevier Science Ltd 2002

spin ½. As shown schematically in Fig. 1a, the overall electronic state is then an antiferromagnetic Mott insulator because Coulomb repulsion prevents electron hopping from Cu to Cu and the exchange correlation is antiferromagnetic in sign.

Doping these insulating CuO_2 layers with holes (or electrons) causes the appearance of new electronic ordered states including HTS. This is because, with doping, hopping of electrons from Cu to Cu becomes possible – as shown in Fig. 1b. A schematic phase diagram of hole-doped cuprates (which are the most widely studied examples of the cuprate HTSs) is shown in Fig. 2. They exhibit T_c of up to 150 K at 'optimum' hole-doping near p ~0.2, where p is the number of doped holes per Cu atom. Microscopically, the cuprate HTSs exhibit many important differences from conventional superconductors. For example, the 'normal' state above T_c is not a metal but the mysterious 'pseudogap' phase[3], the superconducting OP is believed to have $d_{x^2-y^2}$ symmetry[4,5] and the characteristic distance scales (the inter-atomic distance a_0 = ~0.3 nm, the Fermi wavelength λ_F = ~1 nm, and the superconducting coherence length ξ = ~1.5 nm) are all equivalent to each other. No widely accepted microscopic mechanism has been identified to explain superconductivity in the cuprates.

STM: constant-current imaging and tunneling spectroscopy

We study the electronic structure of these materials directly at the atomic scale. For such studies, we use a custom-built[6] low temperature scanning tunneling microscope (STM) that can simultaneously image the surface topography and measure the local density of electronic states (LDOS). Surface preparation consists of cleaving single crystals in cryogenic ultrahigh vacuum (UHV) at temperatures less than ~30 K followed by immediate insertion onto the STM head.

Most of our studies have been carried out on $Bi_2Sr_2CaCu_2O_{8+x}$ (Bi-2212), whose unit cell is shown in Fig. 3. Single crystals of Bi-2212 typically cleave at the weak bonds between the BiO layers to expose a BiO surface. Typical topographic images of this crystal surface are shown in Fig. 4. Fig. 4a shows an 800 Å square field of view (FOV) topographic image of the BiO surface. It is clean and flat and without apparent adatoms. The mottled appearance is a real effect of inhomogeneous superconductivity[7,8] and does not represent surface damage. The atoms are displaced from their

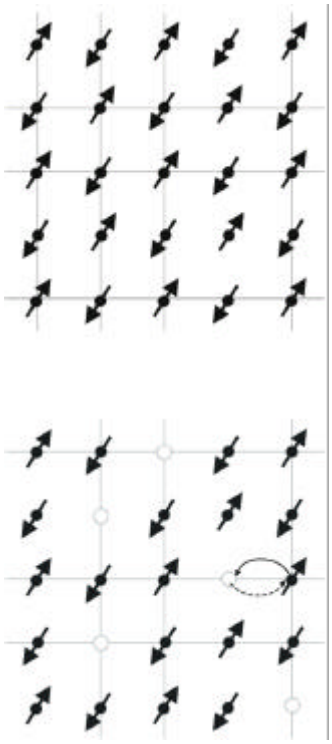

Fig. 1 A model for the relevant electronic degrees of freedom in the CuO_2 plane of the cuprates. (a) Square lattice with one spin ½ state at every vertex. Coulomb repulsion prevents hopping and AF correlations impose an overall AF ground state. (b) With 15% hole doping hopping becomes possible.

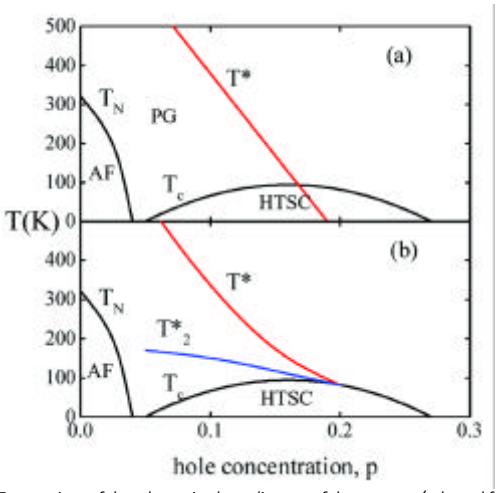

Fig. 2 Two versions of the schematic phase diagram of the cuprates (adapted from [3]).

ideal orthorhombic lattice sites, forming a well-known three dimensional supermodulation[9] of wavelength ~26 Å along the b-axis. This can be discerned as a corrugation of the surface whose maximum vertical displacement appears bright. Fig. 4b is a 275 Å square FOV topograph in which one can begin to see the individual Bi atoms in a square lattice.

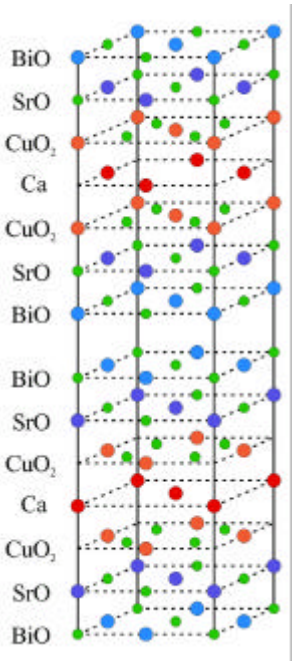

Fig. 3 The unit cell of Bi-2212.

The supermodulation is now clearly evident, as well as an additional apparent redistribution of the atoms away from their expected sites along its spine. Fig. 4c is a 64 Å square FOV topograph in which each individual atom is clearly seen. The all-important Cu atoms lie approximately 5 Å below each Bi atom.

With this STM system, spectroscopic measurements can be made simultaneously with topographic imaging. To do so, the differential tunneling conductance of the vacuum-junction between tip and sample, G(V) = dI/dV, is measured as a function of sample bias voltage V. Because G(V) is proportional to the LDOS at energy E = eV, i.e. LDOS (E = eV) ∝ G(V), the spatial distribution of local density of states can be imaged. This is done by measuring G as a function of V and position (x, y) – a process which we refer to as a spectral-survey. This technique requires extreme stability of the instrument since it takes up to 48 hours, during which register to the crystal surface with atomic resolution cannot be lost.

Bi-2212 is believed to have a $d_{x^2-y^2}$ order parameter symmetry[5]. The ideal k-space dependence of Δ in such a system is shown schematically in Fig 5a. When the magnitude of Δ is averaged around the Fermi surface, the resulting density of quasiparticle states as a function of energy has the form shown in Fig 5b. A very common form

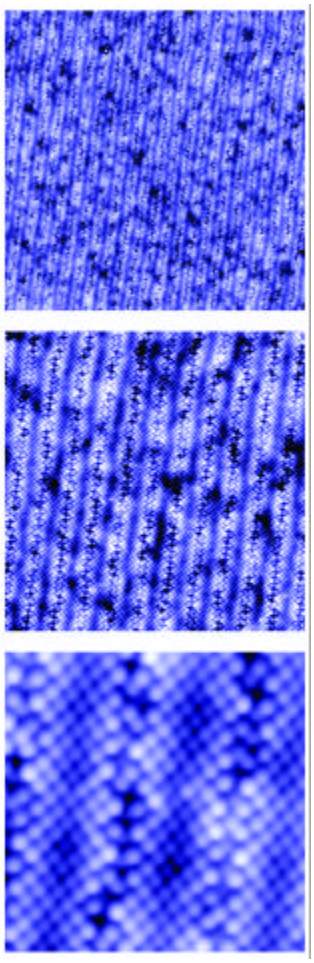

Fig. 4(a) An 800 Å square topographic image of the BiO plane of Bi-2212. (b) 275 Å square topographic image. (c) 64 Å square topographic image.

for the measured G(V) on the BiO plane of Bi-2212 is shown in Fig 5c. It is apparent that this function, which is the central observable of our studies, has many of the attributes expected for the d-wave gap structure. Although the hopping/tunneling process, which allows the electron from the CuO_2 plane to reach the tip, has not been fully determined, we believe that the dI/dV spectra measured in these studies represent primarily the LDOS of the CuO_2 plane.

Electronic impurity-states: theory

A single impurity atom, substituted for Cu in the CuO_2 plane, strongly disrupts the surrounding electronic environment and especially the electronic correlations between electrons on neighboring Cu atoms. The effects of this disruption on HTS can, in principle, be used to help identify the microscopic

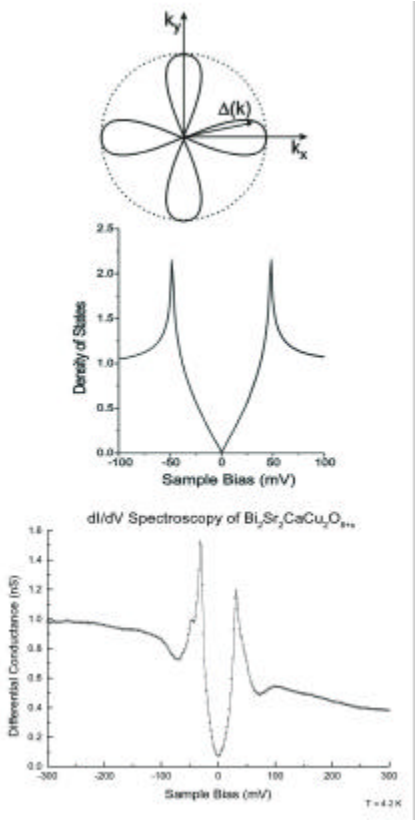

Fig. 5(a) Schematic of the superconducting energy gap in k-space. (b) Theoretically expected local density of states spectrum for a d-wave superconductor. (c) Commonly observed dI/dV spectrum on BiO plane of Bi-2212.

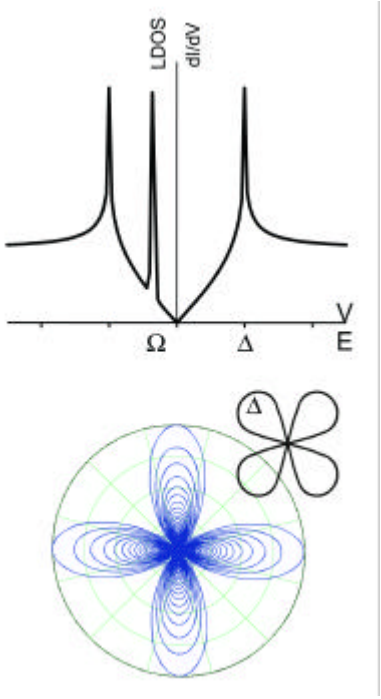

Fig. 6(a) Schematic of the theoretically predicted dI/dV spectrum at the site of an impurity atoms in a d-wave superconductor. (b) Schematic of the theoretically predicted spatial structure of the LDOS near an impurity at the resonance energy Ω in a d-wave superconductor.

mechanism. For this reason, numerous theoretical studies have analyzed the local effects of an impurity atom on the superconducting order parameter, and on the spatial dependence of the quasi-particle LDOS, in a d-wave superconductor.

d-wave BCS models

BCS models with a $d_{x^2-y^2}$ OP predict that quasiparticle scattering at an impurity atom should result in a local scattering resonance[10-25] that, for brevity, we will refer to as an impurity-state. Such impurity-states have been analyzed for both potential (non-magnetic) [10,12-14,16,17,20,22-24] and magnetic[14,20-25] scattering, and can be thought of as almost localized quantum orbitals of well defined energy, Ω, and spatial structure. In this type of model, potential scattering is represented by an additional Coulomb energy U for an electron to hop onto the impurity site. The magnetic interaction between quasiparticle and the moment of an impurity atom is modeled as having energy $W = J\,S\cdot s$ where S is the classical spin of the impurity atom, s is the quasi-particle spin, and J is the exchange energy. If $|U|>|W|$, the solution for the energy of the impurity-state can be written approximately as[14]

$$\frac{\Omega_\pm}{\Delta_0} = \frac{-1}{2N_F(U \pm W)\ln\left|(8N_F(U \pm W)\right|} \qquad (1)$$

Here Δ_0 is the maximum magnitude of the superconducting gap and N_F is the normal density of states per site at the Fermi energy. Thus, at each impurity atom, there should be at least one intra-gap peak in the LDOS at Ω, as shown schematically in Fig 6a. Furthermore, in spatial structure, this impurity-state should be four-fold symmetric and oriented with the nodes of the gap. This is represented schematically in Fig 6b.

Impurity-states: experiment

Ni and Zn atoms are adjacent to Cu in the periodic table. Substitutions of these atoms can be made for up to almost 2% of the Cu atoms in Bi-2212 without altering the crystal (although HTS is suppressed with rising substitution density)[33]. These elements are the most widely used in substitution atom studies in the cuprates.

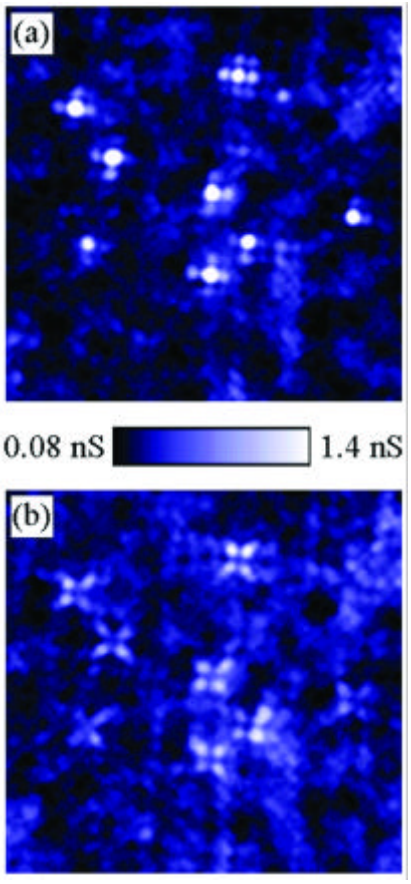

Fig. 7 Two 128 Å square differential conductance maps of Ni doped BSCCO at sample-bias (a) + 9 mV, showing the '+-shaped' regions of high local density of states (LDOS) associated with the Ni atoms and (b) -9 mV, showing the 45° spatially rotated 'X-shaped' pattern. In such an LDOS map, states associated with positive sample-bias are referred to as particle-like, while those at negative sample-bias are hole-like. There are approximately eight Ni atom sites in the field of view. The junction resistance was 1 GΩ at -100 mV for both maps and all data reported in this paper were acquired at 4.2 K.

Ni substituted for Cu in Bi-2212[26]

We use $Bi_2Sr_2Ca(Cu_{1-x}Ni_x)_2O_{8+d}$ single crystals, grown by the floating-zone technique[27]. These crystals have x = 0.005 with T_c = 83 K and x = 0.002 with T_c = 85 K, respectively. The Ni atoms substitute for Cu in the superconducting CuO_2 plane and are believed to be in the Ni^{2+} $3d^8$ electronic state with spin S = 1, as compared to the Cu^{2+} $3d^9$ S = ½ state of Cu. Above T_c each Ni atom possesses a strong magnetic moment of approximately 1.5 μ_B[28]. Therefore, we might expect Ni to be a magnetic scatterer and, since magnetic scattering is highly destructive to singlet Cooper pairs, to destroy superconductivity locally.

Fig. 7 shows two simultaneously acquired LDOS maps from Ni-doped samples measured at sample bias V = ±9 mV. They reveal both the particle-like (positive-bias) and hole-like (negative-bias) components of one of the impurity-states that exist at each Ni atom. At +9 mV there exist '+-shaped' regions of higher LDOS, while at the same locations but at -9 mV the corresponding higher LDOS regions are 'X-shaped'. LDOS maps at V = ±19 mV reveal the particle-like and hole-like components of a second impurity-state whose spatial structure is very similar to that at V = ±9 mV.

We believe these phenomena are associated with the Ni atoms for several reasons. First, from the unit cell shown in Fig. 3, one can see that the Cu site where the Ni dopant atom would reside is directly below a surface Bi atom (but separated from it by the intervening SrO_2 layer). Correlations between topographies and LDOS maps show that all the impurity-states of the form shown in Fig. 7 are indeed centered at Bi sites. Furthermore, the density of the observed impurity-states is in reasonable agreement with the nominal Ni doping concentrations and, finally, features like those in Fig. 7 have never been observed in non-Ni-doped crystals.

High-resolution ±9 mV LDOS maps of the Ni impurity-states (Figs. 8a and 8b) acquired simultaneously with a topographic image of the BiO surface (Fig. 8c) show in detail how an impurity-state consists of two spatially complementary components, i.e. particle-like LDOS is high in regions where the hole-like LDOS is low, and vice versa. To illustrate these relationships, Fig. 8d shows a schematic diagram of the relative locations of Cu atoms, the orientation of the $d_{x^2-y^2}$ OP, and the location of the particle-like (green) and hole-like (purple) components of the impurity-state.

We also measure the energy dependence of the spectra near Ni atoms. Fig. 9 shows typical dI/dV spectra taken at locations above the Ni atom, above the first nearest neighbour (1-NN) and second nearest neighbor (2-NN) Cu atoms, at a distance of 30 Å from the impurity site, and the average spectrum for the whole impurity-state region. Two particle-like LDOS peaks are observed at each Ni site. The average magnitudes of these impurity-state energies are Ω_1 = 9.2 ±1.1 meV and Ω_2 = 18.6 ±0.7 meV. Both these peaks become hole-like at all the 1-NN Cu sites and again particle-like at the 2-NN Cu sites but, overall, the spatially averaged spectrum for this whole impurity-state (shown in Fig. 9b) remains very close to particle-hole symmetric.

Several deductions can be made from these data. First, the two on-site LDOS peaks reveal that there are two distinct impurity-states associated with each Ni atom. This can be explained by theories that consider both potential and

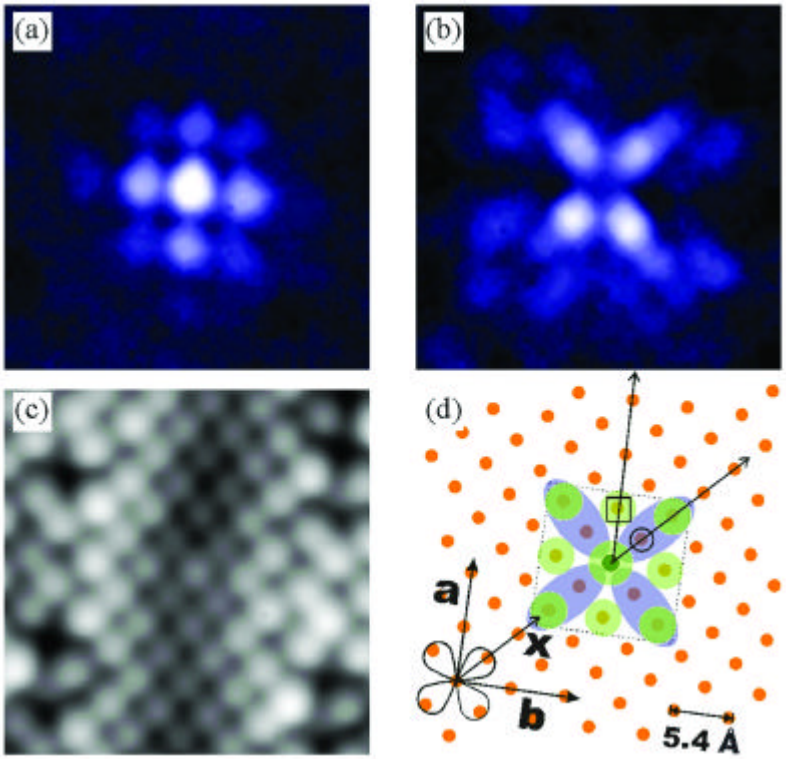

Fig. 8 (a, b) 35 Å square differential conductance maps of an Ni atom at (a) +9 mV and (b) -9 mV. (c) A 35 Å square atomic resolution topograph of the BiO surface obtained simultaneously with the maps. (d) Using the information in (a), (b) and (c) and the fact that the Cu atoms in the CuO_2 plane lie directly beneath the Bi atoms in the BiO plane, we draw a schematic showing the relative position of the Ni atom (black solid circle) with respect to the Cu atoms (orange solid circles) in the CuO_2 plane. Also depicted is the orientation of the $d_{x^2-y^2}$ OP, and the positions of the 1-NN (open circle) and 2-NN (open square) atoms where the spectra shown in Fig. 3 are acquired. The 10 Å square region inside which the spatial integration of the whole impurity-state LDOS was carried out is also shown. The junction resistance is 1 G Ω at –100 mV for all data.

magnetic interactions. Potential scattering generates a single spin-degenerate impurity-state[12-14,16,17,19-23]. Any additional magnetic interactions between an impurity moment and the quasiparticle spin lift the spin-degeneracy, creating two spin-polarized impurity-states at each magnetic impurity atom[14]. This is in good qualitative agreement with the data.

As shown in Figs. 8 and 9, the spectral weight of an impurity-state oscillates between particle-like and hole-like as a function of distance from the Ni atom, but the average spectrum of the impurity-state is particle-hole symmetric. Such overall particle-hole symmetry is expected if superconductivity is not disrupted[20,22-24,29,30] and calculations for the d-wave impurity-state wavefunction show that the particle-like and hole-like LDOS should be spatially complementary[20,22-24]. In addition, as shown in Fig. 10, the superconducting gap magnitude (as deduced from the energy of the coherence peaks) does not change as we approach the impurity site. All these observations point to the fact that HTS is not disrupted locally by the magnetic moment of Ni – a quite surprising result.

In summary, two local states in qualitative agreement with d-wave impurity scattering theory can be identified at each Ni impurity atom. Analysis of the Ni impurity-state energies by substituting the measured values of Ω_1 and Ω_2 and Δ_0 = 28 meV into Equation 1, we find $N_F U$ = -0.67 and $|N_F W|$ = 0.14. This identifies the dominant effects of Ni as due to potential, not magnetic, scattering. Nonetheless, the presence of two impurity-states indicates that the Ni atom possesses a magnetic moment, which lifts the spin degeneracy generating two spin-polarized excited states. The existence and structure of the particle-like to hole-like oscillations and the constant gap magnitude indicate that superconductivity is nowhere disrupted.

Zn substituted for Cu in Bi-2212[31]

The $Bi_2Sr_2Ca(Cu_{1-x}Zn_x)_2O_{8+d}$ single crystals used for studies of Zn substitution are also grown by the floating zone

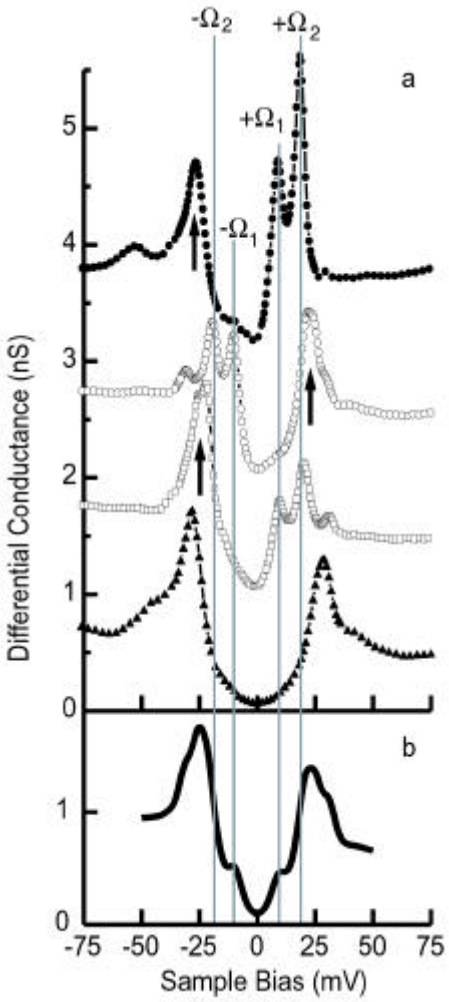

Fig. 9 Differential conductance spectra obtained at four positions near the Ni atom showing the resonances at $\pm\Omega_1$ and $\pm\Omega_2$ and the superconducting coherence peaks. These curves are shifted from each other by 1 nS for clarity. (a) The spectrum above the Ni atom site (solid circles), above the first nearest neighbor Cu atom position (open circles), above the second nearest neighbor Cu atom (open squares), and a typical spectrum 30 Å from an impurity atom (solid triangles). The location of the Ni atom along with the 1- and 2-NN is shown schematically in Fig. 8. (b) The average of conductance spectra over a 10 Å square area centered on an Ni atom, showing the particle-hole symmetric nature of the spatially integrated LDOS. The junction resistance was 1 GΩ at -200 mV for all spectra.

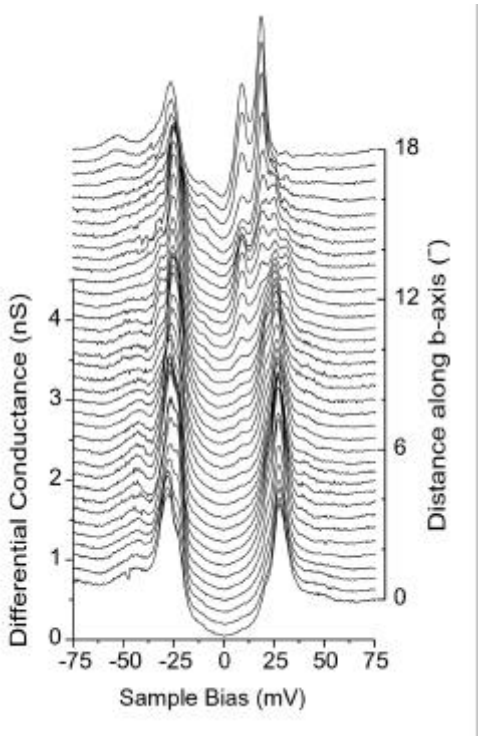

Fig. 10 A series of differential conductance spectra, taken as a function of distance away from the center of an Ni impurity-state along the b-axis. The top spectrum is taken above the Ni site. The spectra, each separated by 0.5 Å, show that over a ~20 Å range the magnitude of the superconducting gap $\Delta_0 = 28$ meV, as measured by the distance from the hole-like coherence peak to the Fermi level, is not suppressed in the presence of the Ni impurity. This study was carried out in a region with constant Δ_0 of 28 meV. The junction resistance was 1 GΩ at -100 mV for all spectra.

method[32] and have x = 0.6% nominal doping concentration of Zn[27]. They have a T_c of 84 K with a transition width of 4 K. The Zn atoms substitute for Cu and are believed to be in the Zn^{2+} $3d^{10}$ electronic state with spin S = 0.

Fig. 11b shows a typical LDOS map taken at sample bias -1.5 meV on Zn-doped Bi-2212, whose topograph is shown in Fig. 11a. A number of randomly distributed impurity-states with high LDOS and a distinct four-fold symmetry are observed. These are the impurity-states equivalent to, but in detail very different from, those in Ni-doped Bi2212 in Fig. 7. There is also a signal at these locations at Ω = +1.5 meV but, because it is at least two orders of magnitude weaker than that at Ω = -1.5 meV, we do not regard it as a particle-like component of the Zn impurity-state.

In Fig. 12 we show the differences between conductance spectra taken exactly at the centers of these Zn impurity-states and spectra taken at regular superconducting regions of the sample (dark areas in Fig. 11). At a Zn atom we see that the coherence peaks are almost completely destroyed and a narrow, intense peak in the LDOS occurs at -1.5 meV.

We again identify these impurity-states as being due to the Zn atoms via comparison between pairs of high resolution topographic and LDOS images, which show that the center of an impurity-state always coincides with the site of a surface Bi atom that is above the Cu site. Furthermore, the density of the observed scattering resonances is x = 0.2 ±0.1 %, in reasonable agreement with the nominal Zn doping concentration.

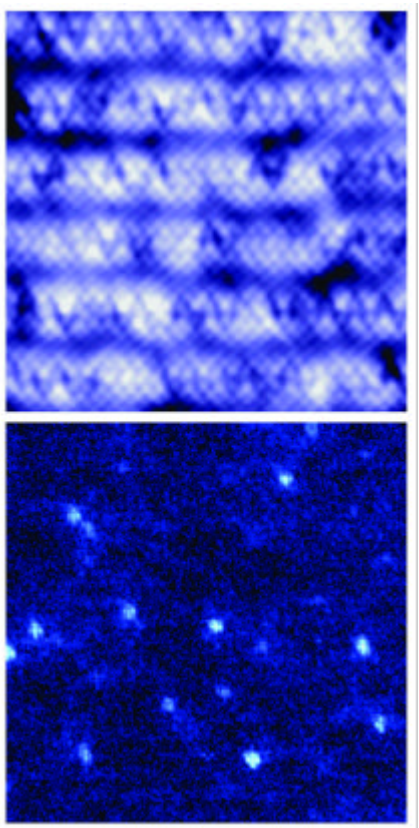

Fig. 11(a) A 560 Å square constant current topograph of a Zn-BSCCO single crystal. (T = 4.2 K, I = 100 pA, V_{sample} = -100 mV). (b) A 560 Å square differential tunneling conductance map taken at sample bias V_{sample} = 0 on the same surface (with the same orientation) as that shown in Fig. 11a. The Zn scattering sites appear as bright regions of approximate dimension 15 Å, each clearly exhibiting a cross-shaped four-fold symmetric structure. To acquire this image we operate at 4.2 K, set a 1 GΩ junction resistance (I = 200 pA, V_{sample} = -200 mV), and measure the conductance with a standard low frequency ac lock-in technique ($A_{modulation}$ = 500 μV_{rms}, $f_{modulation}$ = 447.3 Hz).

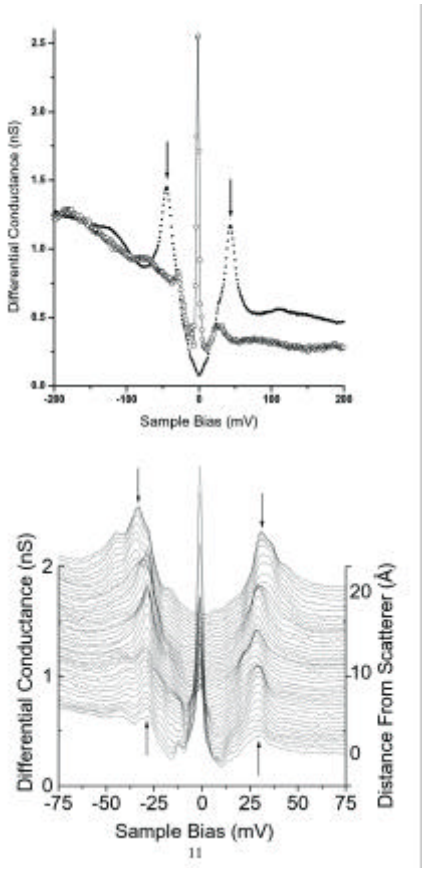

Fig. 12(a) Differential tunneling conductance versus sample bias taken at two different locations on the Zn-Bi2212 crystal. The spectrum of a 'regular' superconducting region of the sample, where Zn scatterers are absent, is shown as the solid circles. The superconducting coherence peaks are indicated by the arrows. The data shown as open circles, with an interpolating fine solid line, is the spectrum taken exactly at the center of impurity-state. It shows both the intense scattering resonance centered at Ω = -1.5 mV, and the very strong suppression of the superconducting coherence peaks and gap magnitude at this same location. (b) A series of tunneling spectra taken on a line from the scatterer along the b-axis direction in 0.5 Å steps. This clearly shows suppression of the coherence peaks (whose absence at the Zn scatterer is indicated by upward pointing arrows), and recovery of the superconductivity (along with the coherence peaks whose presence is indicated by downward pointing arrows) within a distance of ~15 Å from the scattering site.

Fig. 13a shows the topography of the surface at a Zn impurity-state. Fig. 13b is an LDOS map centered on Zn, which is presented in a logarithmic intensity scale. In this representation we see that, in addition to the central peak, a dominant feature is a relatively bright cross-shaped region aligned along the crystal a- and b-axes, and extending to a radius of about 10 Å. Concentric with this bright cross, and rotated 45° relative to it, another cross-shaped feature with considerably lower intensity extends to approximately 30 Å from the center. We show schematically in Fig. 13c the positions of the Cu and O atoms in the CuO_2 plane, with the relative positions of the LDOS maxima overlaid as heavy circles, as well as the orientations of the d-wave gap nodes. Analysis of the simultaneously imaged atomic positions and LDOS intensities in Figs. 13a and 13b indicate that the positions of the four nearest-neighbor Cu atoms to the Zn have no local LDOS maxima associated with them, while the positions of the eight 2-NN and 3-NN Cu atoms coincide with local maxima in the LDOS and appear to form a 'box' around the scatterer, as seen in Fig. 13b.

The Zn atom affects the magnitude of the coherence peaks and the width of the superconducting gap, as shown in Fig. 12b. This is a plot of the measured evolution of the complete LDOS spectrum as the tip is moved away from the scattering site along the b-axis. The superconducting coherence peaks are strongly suppressed at the Zn scattering site and recover to their bulk value over a distance of about 15 Å.

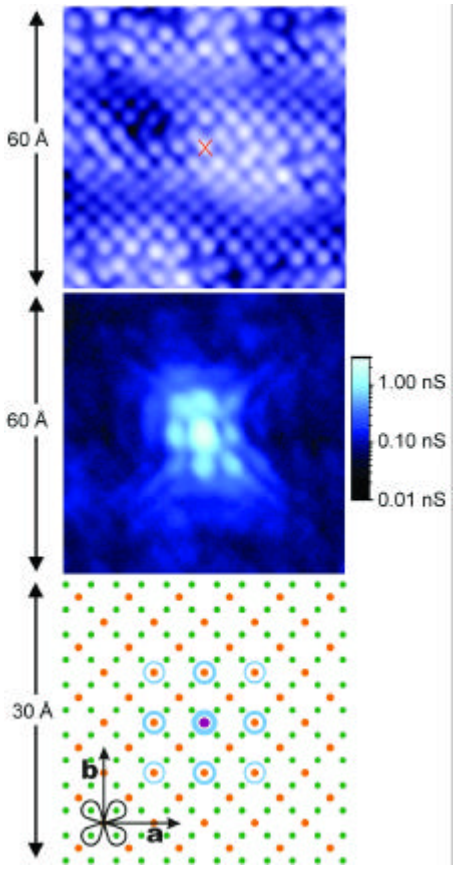

Fig. 13(a,b) Simultaneously acquired, 60 Å square, high spatial resolution images of the topography and the differential conductance at V_{sample} = -1.5 mV and at V_{sample} = +1.5. The bright center of the impurity state is located at the position of the Bi atom marked by an 'X' in Fig. 13a. The inner bright cross is oriented with the nodes of the d-wave gap (as indicated schematically in Fig. 13c). The weaker outer features, including the ~30 Å long 'quasi-particle beams' at 45° to the inner cross, are oriented with the gap maxima. (c) This is a 30 Å square schematic representation of the square CuO_2 lattice, showing its relative orientation to the BiO surface. The Cu atoms are indicated as large solid circles and the O atoms as small solid circles, while the Zn scatterer is at the central point. The crystal a- and b-axis orientations, and the orientations of the maxima and nodes of the d-wave superconducting gap are also shown. The location of the maxima in the LDOS, as measured from Fig. 13b, are shown schematically as heavy circles surrounding the atomic sites with which they appear to be associated. The intensity of the LDOS at these sites is shown schematically by the thickness of the line.

The strength of the quasiparticle scattering leading to these Zn impurity-states, in terms of scattering phase shift $\delta_0 = \tan^{-1}(\pi N_F U)$, δ_0 may be calculated[12] using the ratio of the resonance energy Ω to the energy gap Δ_0 in Equation 1. Using an average gap value (away from the impurities) of Δ_0 = 44 mV and Ω = -1.5 mV, we obtain a phase shift of 0.48π. This confirms that scattering from Zn is very close to the unitary limit ($\delta_0 = \pi/2$)[10-19]. The predicted particle-hole symmetry is, however, absent when averaging over the whole impurity-state. The predicted four-fold symmetry in the LDOS, and its alignment with the d-wave gap nodes, near an impurity atom are, however, observed.

In summary, one local state can be identified at each Zn impurity atom. Only one peak in LDOS is detected at each Zn atom and it occurs at an energy Ω = -1.5 ±0.5 mV so particle-hole symmetry is absent in this impurity-state. At these sites, the superconducting coherence peaks are strongly suppressed, indicating the almost complete local destruction of superconductivity by Zn.

Analysis

D-wave BCS models are unlikely to capture the full atomic-scale correlated electron physics of the cuprates. Nonetheless, they have proven quite successful in the identification of the general class of phenomena to be observed at impurity atoms in these materials. For example, the central set of proposals that quasi-particle scattering resonances, and localized impurity-states characteristic of the OP symmetry, could be created by individual impurity atoms in a d-wave superconductor are correct.

Bi-2212

Among the many surprises in the data are the clear differences between nanoscale electronic phenomena seen at Zn and Ni impurity atoms. Previous experimental studies using these two impurities have revealed two apparently contradictory aspects of their effects on HTS. On one hand, resistivity[33,34], microwave surface resistivity[35], and T_c[33,34] measurements show quite similar dependences on Zn and Ni doping densities. On the other hand, probes sensitive to magnetic phenomena such as NMR[36-42] and inelastic neutron scattering (INS)[43], and probes of the superfluid density such as penetration depth[35] and muon-spin-rotation (μSR)[44], show characteristics of Ni- and Zn-doped samples that are dramatically different.

From the direct information on their electronic effects, the apparent conflicts between results from different probes can be reconciled. The first set of probes is sensitive to quasiparticle scattering. Calculation of the potential scattering phase shift $\delta_0 = \tan^{-1}(\pi N_F U)$ for Ni gives $\delta_0 = 0.36\pi$ while Zn is a unitary scatterer ($\delta_0 \approx \pi/2$). The similarity of these phase shifts implies that phenomena dependent on scattering should be quite similar in Ni- and Zn-doped samples. In an Abrikosov-Gorkov model, using these parameters yields a T_c suppression only about 20% faster by Zn than by Ni, certainly within the range of experimental observations[33,34].

Among the second set of measurement techniques are those sensitive to superconductivity itself. For example, penetration depth[35] and μSR[44] measurements show that, in the bulk, Zn strongly depletes superfluid density, but Ni has a much weaker impact. The STM data provide a microscopic explanation for these differences – Zn atoms locally destroy superconductivity while Ni atoms do not.

Finally, magnetic probes sensitive to spin fluctuations reveal dramatic changes with Zn-doping[36,38-43], but only weak perturbations with Ni-doping[36,37,41,43]. Explanations for these phenomena have been proposed[39,40,42] whereby Zn behaves like a 'magnetic hole' (a spinless site in an environment of strongly exchange-coupled spins) that dramatically alters Cu-Cu exchange correlations and thereby disrupts superconductivity. By contrast Ni is believed to retain a magnetic moment that barely perturbs the antiferromagnetic exchange correlations, which facilitate superconductivity. While the NMR and INS data[36-43] are quite consistent with the magnetic component of such models, their predictions for local electronic phenomena at Ni and Zn impurities can now be tested. The STM data demonstrate that, despite their magnetic moments, scattering at Ni atoms is dominated by potential interactions and furthermore, whereas Zn atoms locally destroy superconductivity within a 15 Å radius, the magnetic Ni atoms coexist with unweakened superconductivity. All these observations are consistent with this microscopic picture developed from the magnetic probes.

Conclusions

These data reveal the beauty and complexity of the atomic scale electronic/magnetic structure that can occur in the cuprates. They confirm many of the preliminary expectations for individual impurity atom phenomena in a d-wave superconductor. They also represent a precise series of atomic scale phenomena whose details should be predictable within a correct microscopic theory for HTS and, as such, will act as a stringent test of candidates for that theory.

Acknowledgments

I wish to acknowledge and thank my collaborators Hiroshi Eisaki, Eric W. Hudson, Jenny Hoffman, Kristine M. Lang, Vidya Madhavan, Kyle McElroy, Shuheng H. Pan, Raymond W. Simmonds, and Shin-ichi Uchida. Over the past nine years this work has been supported by the LDRD Program of the Lawrence Berkeley National Laboratory under the Department of Energy Contract No. DE-AC03-76SF00098, the CULAR Program of the Los Alamos National Laboratory, the Office of Naval Research, the National Science Foundation, Grant-in-Aid for Scientific Research on Priority Area, a COE Grant from the Ministry of Education (Japan), and a grant from NEDO (Japan).

REFERENCES

1. See for example: J.R. Schrieffer, Theory of superconductivity (1964), W.A. Benjamin, New York
2. See for example: M. Tinkham, Introduction to superconductivity (1975) McGraw-Hill, New York
3. Tallon, J. L., and Loram, J. W., Physica C (2001) 349, p.,53
4. Van Harlingen, D. J., Rev. Mod. Phys. (1995) 67, p. 515-535
5. Tsuei, C. C., and Kirtley, J. R., Rev. Mod. Phys. (2000) 72, p. 969-1016
6. Pan, S.H., et al., Rev. Sci. Inst. (1999) 70, p. 1459-1463
7. Pan, S. H., et al., Nature (2001) 413, p. 282
8. Lang, K. M., et al., Nature (2002) 415, p. 412
9. Gao, Y., et al., Science (1988) 241, p. 954
10. Lee, P.A., Phys. Rev. Lett. (1993) 71, p. 1887-1890
11. Byers, J.M., et al., Phys. Rev. Lett. (1993) 71, p. 3363-3366
12. Balatsky, A.V., et al., Phys. Rev. B (1995) 51, p. 15547-15551
13. Salkola, M.I., et al., Phys. Rev. Lett. (1996) 77, p. 1841-1844
14. Salkola, M.I., et al., Phys. Rev. B (1997) 55, p. 12648-12661
15. Hirschfeld, P.J., and Puttika, W.O., Phys. Rev. Lett. (1996) 77, p. 3909-3912
16. Franz, M., et al., Phys. Rev. B (1996) 54, p. R6897-6900
17. Salkola, M.I. and Schrieffer, J.R., Phys. Rev. B (1998) 58, p. R5952-5955
18. Atkinson, W.A., and MacDonald, A.H., Science (1999) 285, p. 57-58
19. Flatté, M.E., and Byers, J.M., Solid State Physics (1999) 52, p. 137-228
20. Flatté, M.E., and Byers, J.M., Phys. Rev. Lett. (1998) 80, p. 4546
21. Tsuchiura, H., et al., Phys. Rev. Lett. (2000) 84, p. 3165-3168
22. Flatté, M.E., Phys. Rev. B (2000) 61, p. R14920-14923
23. Haas, S., and Maki, K., Phys. Rev. Lett. (2000) 85, p. 2172-2175
24. Martin, I., et al., cond-mat/ 0012446 (2000)
25. Zhang, G.-M., et al., Phys. Rev. Lett. (2001) 86, p. 704-707
26. Hudson, E.W., et al., Nature (2001) 411, p. 920
27. We are greatly indebted to H. Eisaki and S. Uchida for the provision of these samples
28. Mendels, P. et al., Physica C (1994) 235, p. 1595-1596
29. Yazdani, A., et al. Science (1997) 275, p. 1767-1770
30. Flatté, M.E., and Byers, J.M., Phys. Rev. Lett. (1997) 78, p. 3761-3764
31. Pan, S.H., et al., Nature (2000) 403, p. 746
32. Motohira, N., et al., J. Ceram. Soc. Jpn. (1989), 97, p. 944-950
33. Maeda, A., et al., K. Phys. Rev. B (1990) 41, p. 4112-4117
34. Kuo, Y.K., et al., Phys. Rev. B (1997) 56, p. 6201-6206
35. Bonn, D.A., et al., Phys Rev. B (1994) 50, p. 4051-4063
36. Ishida, K., et al., J. Phys. Soc. Jpn. (1993) 62, p. 2803-2818
37. Tokunaga, Y., et al., K. Solid State Comm. (1997) 103, p. 43-47
38. Mahajan, A.V., et al., J.F Phys. Rev. Lett. (1994) 72, p. 3100-3103
39. Bobroff, J., et al., Phys. Rev. Lett. (1999) 83, p. 4381-4384
40. Bobroff, J., et al., Phys. Rev. Lett. (2001) 86, p. 4116
41. Williams, G.V.M., et al., R. Phys. Rev. B (2000) 61, p. 4319-4325
42. Julien, M.-H., et al., Phys. Rev. Lett. (2000) 84, p. 3422-3425
43. Sidis, Y., et al., Phys. Rev. Lett. (2000) 84, p. 5900-5903
44. Bernhard, C., et al., Phys. Rev. Lett. (1996) 77, p. 2304-2307